This article was downloaded by: [Siauliu University Library]
On: 17 February 2013, At: 06:51
Publisher: Taylor & Francis
Informa Ltd Registered in England and Wales Registered Number: 1072954
Registered office: Mortimer House, 37-41 Mortimer Street, London W1T 3JH, UK

Advanced Composite Materials
Publication details, including instructions for authors and subscription information:
http://www.tandfonline.com/loi/tacm20

Fatigue Simulation for Ti/GFRP Laminates using Cohesive Elements

T. Yamaguchi [a] , T. Okabe [b] & T. Kosaka [c]
[a] Department of Aerospace Engineering, Tohoku University, Japan
[b] Department of Aerospace Engineering, Tohoku University, Japan;, Email: okabe@plum.mech.tohoku.ac.jp
[c] Graduate School of Engineering, Osaka City University, Japan
Version of record first published: 02 Apr 2012.

To cite this article: T. Yamaguchi , T. Okabe & T. Kosaka (2010): Fatigue Simulation for Ti/GFRP Laminates using Cohesive Elements, Advanced Composite Materials, 19:2, 107-122

To link to this article: http://dx.doi.org/10.1163/092430410X490428

PLEASE SCROLL DOWN FOR ARTICLE

Full terms and conditions of use: http://www.tandfonline.com/page/terms-and-conditions

This article may be used for research, teaching, and private study purposes. Any substantial or systematic reproduction, redistribution, reselling, loan, sub-licensing, systematic supply, or distribution in any form to anyone is expressly forbidden.

The publisher does not give any warranty express or implied or make any representation that the contents will be complete or accurate or up to date. The accuracy of any instructions, formulae, and drug doses should be independently verified with primary sources. The publisher shall not be liable for any loss, actions, claims, proceedings, demand, or costs or damages whatsoever or

howsoever caused arising directly or indirectly in connection with or arising out of the use of this material.

Downloaded by [Siauliu University Library] at 06:51 17 February 2013

VSP

Advanced Composite Materials 19 (2010) 107–122

ADVANCED COMPOSITE MATERIALS
brill.nl/acm

Fatigue Simulation for Ti/GFRP Laminates using Cohesive Elements

T. Yamaguchi [a], **T. Okabe** [a,*] **and T. Kosaka** [b]

[a] Department of Aerospace Engineering, Tohoku University, Japan
[b] Graduate School of Engineering, Osaka City University, Japan

Received 20 December 2008; accepted 23 March 2009

Downloaded by [Siauliu University Library] at 06:51 17 February 2013

Abstract
Hybrid laminates made of polymer matrix composite plies with a metal sheet are called fiber metal laminates (FMLs). This study presents a new numerical approach for examining the fatigue damage progress in FMLs. A layer-wise finite element along with a cohesive element are used to predict the fatigue damage progress for splitting, transverse cracking and delamination. Four-node cohesive elements are introduced to express 0° ply splitting and transverse cracking. Eight-node cohesive elements are inserted into the ply interfaces to represent delamination. The most important character of this model is that the proposed simulation introduces a damage-mechanics concept into the degradation process in cohesive elements in order to express the damage progress due to cyclic loading. This enables us to address the complicated fatigue damage process observed in a FML. We applied this model to titanium/glass fiber-reinforced plastic (Ti/GFRP) laminates and compared the simulated results with the experiment data reported in the references. We confirmed that this model can reproduce the fatigue damage process in a FML. The effect of the parameters of the cohesive element on Ti crack growth and the delamination profile were also investigated. The Ti crack-growth rate was found to be strongly associated with the delamination profile near the crack tip.
© Koninklijke Brill NV, Leiden, 2010

Keywords
Fiber metal laminates, fatigue, delamination, cohesive zone elements, finite element method

1. Introduction

Fiber metal laminate (FML), made of polymer matrix composite plies with a metal sheet, is widely used as a fuselage skin material for aircraft. FML is a hybrid material with high fatigue tolerance, specific strength and stiffness, and resistance to impact and lightning strikes [1, 2]. First, aramid fiber/epoxy laminate and aluminum-alloy (ARRAL) was developed. Second, glass fiber-reinforced aluminum laminate (GLARE) was developed and used on the Airbus A380 as a skin

* To whom correspondence should be addressed. E-mail: okabe@plum.mech.tohoku.ac.jp
Edited by the JSCM

© Koninklijke Brill NV, Leiden, 2010
DOI:10.1163/092430410X490428

material for the upper fuselage and the leading edges of the vertical and horizontal tail planes. Third, FML, with a titanium alloy sheet (TiGr) that can endure high temperatures at supersonic operating speeds, was recently developed [3–5]. A detailed understanding of the damage process under an applied load, especially a cyclic load, is needed in order to use FML extensively in engineering applications. However, there is little research that completely explains the fatigue damage progress.

Some researchers have proposed models for the face-sheet crack-growth behavior of FML. Burianek and Spearing [6] predicted the crack-growth rate by using a finite-element method that included delamination at the interface. However, this model could not reproduce the real damage progress seen in experiment results because it incorporated an assumption concerning delamination shape and ignored any damage occurring in the internal FRP layer. Although the face-sheet crack-growth rate provides a guide to the remaining life of the FML, there is no prediction model that considers the delamination profile growth, which closely correlates with the face-sheet crack-growth rate.

This paper proposes a new numerical approach to the fatigue damage progress in a FML that considers multiple damage modes, including face-sheet cracking, delamination, and damage in the internal FRP layer. The structure of this paper is as follows. We first present a formulation of the numerical model, especially as it applies to cohesive elements, and a residual-strength degradation law for cohesive elements that expresses the effects of cyclic loading. We then demonstrate the validity of the simulation by comparing the simulation results with the experiment results recorded by Nakatani *et al.* [8]. Finally, we discuss the effect of the parameters of cohesive elements that express the strength of the bonding ply or interlayer damage on the face-sheet crack-growth rate.

Downloaded by [Siauliu University Library] at 06:51 17 February 2013

2. Model

The following model was used to simulate the damage progress in open-hole Ti/GFRP cross-ply laminates under cyclic loading. The lay-up of the laminate is $[Ti/0_4/90_8]_s$, the same as in the experiment conducted by Nakatani *et al.* [8].

The model is separated into individual layers representing the titanium layer, 0° layer, and 90° layer as seen in Fig. 1. The titanium layer is assumed to be isotropic and each ply of the GFRP laminates is assumed to be an orthotropic homogeneous body. The model consists of linear-elastic, four-node Mindlin plate elements that permit consideration of out-of-plane deformation.

In this modeling, we consider the following damage modes:

- Titanium cracking.
- Splitting (in 0° layer).
- Transverse cracking (in 90° layer).

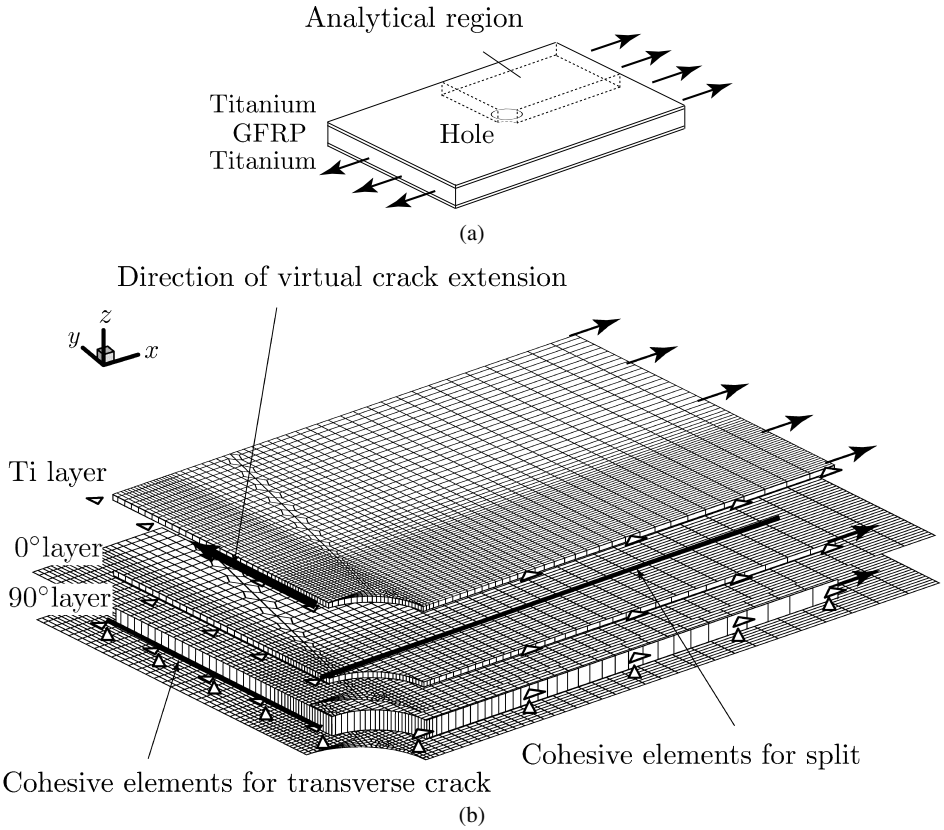

Figure 1. Finite-element model for Ti/GFRP laminate. (a) Schematic of Ti/GFRP laminate. (b) Finite element mesh.

Downloaded by [Siauliu University Library] at 06:51 17 February 2013

- Delamination at the Ti/GFRP interface.
- Delamination at the 0°/90° interface.

Cohesive elements are used to express these damage modes, except for titanium cracking. To introduce the effect of cyclic loading, Kachanov's damage progress law [9] was modified to apply to the residual strength of cohesive elements. Generally, Paris' law is used to represent the crack growth rates of metals. Therefore, the virtual crack closure technique (VCCT) plus Paris' law were used to predict crack growth in the titanium layer.

2.1. Finite-Element Analysis using Cohesive Elements

A cohesive element utilizes the relation between traction and relative displacement of the crack surface, as illustrated in Fig. 2. The relation between the traction $\mathbf{T}$ and the relative displacement $\boldsymbol{\Delta}$ is defined using the residual-strength parameter for the

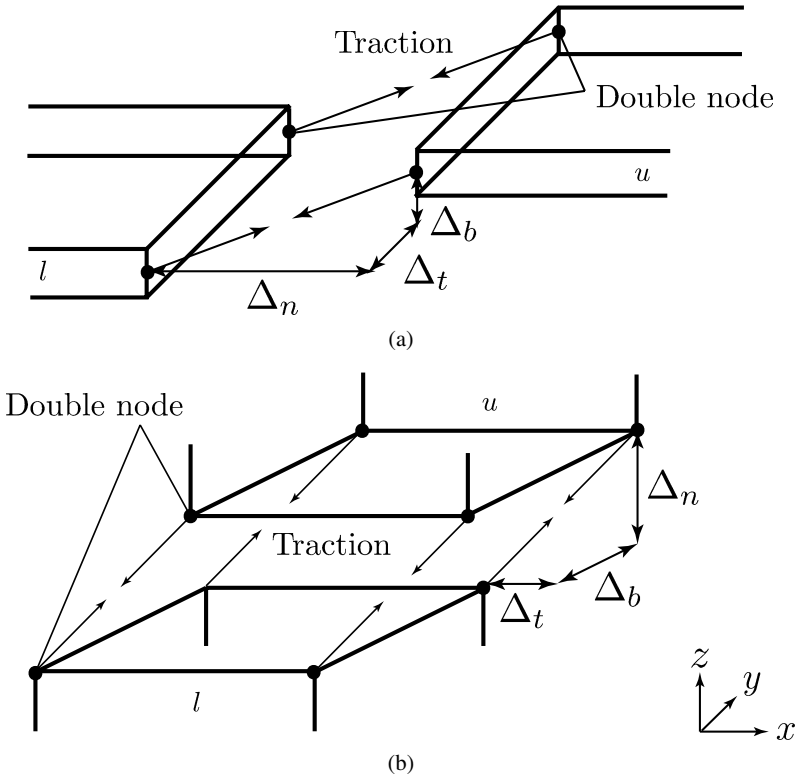

Figure 2. Cohesive zone model. (a) 4-Node cohesive element for split and transverse crack. (b) 8-Node cohesive element for delamination.

elements, s, proposed by Geubelle and Baylor [10]:

$$\mathbf{T} = \begin{Bmatrix} T_{\mathrm{n}} \\ T_{\mathrm{t}} \\ T_{\mathrm{b}} \end{Bmatrix} = \begin{bmatrix} \dfrac{s}{1-s}\dfrac{\tau_{\mathrm{n\,max}}}{\Delta_{\mathrm{nc}}} & 0 & 0 \\ 0 & \dfrac{s}{1-s}\dfrac{\tau_{\mathrm{t\,max}}}{\Delta_{\mathrm{tc}}} & 0 \\ 0 & 0 & \dfrac{s}{1-s}\dfrac{\tau_{\mathrm{b\,max}}}{\Delta_{\mathrm{bc}}} \end{bmatrix} \begin{Bmatrix} \Delta_{\mathrm{n}} \\ \Delta_{\mathrm{t}} \\ \Delta_{\mathrm{b}} \end{Bmatrix} = \overline{\mathbf{D}}_{\mathrm{coh}} \boldsymbol{\Delta}. \quad (1)$$

Subscripts n, t and b indicate the cracking modes of normal tensile deformation, in-plane shear, and out-of-plane shear. $\tau_{i\,\max}$ and $\Delta_{i\mathrm{c}}$ ($i = \mathrm{n}, \mathrm{t}, \mathrm{b}$) are the strength and the critical relative displacement in each cracking mode. The term 'strength' represents a criterion for starting the damage process in cohesive elements. The critical relative displacement is the relative displacement with no traction in the cohesive element. At the critical energy release rate, $G_{i\mathrm{c}}$ ($i = \mathrm{I}, \mathrm{II}, \mathrm{III}$), equal to the

Downloaded by [Siauliu University Library] at 06:51 17 February 2013

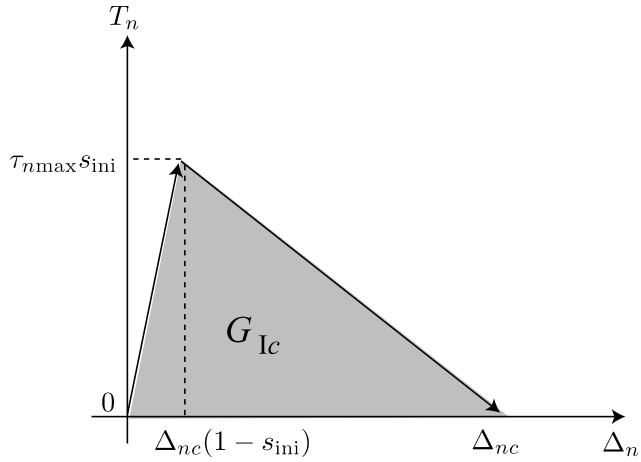

Figure 3. Schematic illustration of the traction-separation laws used in this paper.

area of the shaded region in Fig. 3, the critical relative displacement is defined as follows:

$$\Delta_{\mathrm{nc}} = \frac{2G_{\mathrm{Ic}}}{\tau_{\mathrm{n}\max} s_{\mathrm{ini}}}, \qquad \Delta_{\mathrm{tc}} = \frac{2G_{\mathrm{IIc}}}{\tau_{\mathrm{t}\max} s_{\mathrm{ini}}}, \qquad \Delta_{\mathrm{bc}} = \frac{2G_{\mathrm{IIIc}}}{\tau_{\mathrm{b}\max} s_{\mathrm{ini}}}. \tag{2}$$

Here, s_{ini} is the initial value of parameter s ($s_{\mathrm{ini}} = 0.999$ in this study). Parameter s is calculated as a function of the relative displacements:

$$s = \min[s_{\min}, \max[0, 1 - |\tilde{\Delta}|]], \tag{3}$$

$$\tilde{\Delta} = \{\Delta_{\mathrm{n}}/\Delta_{\mathrm{nc}}, \Delta_{\mathrm{t}}/\Delta_{\mathrm{tc}}, \Delta_{\mathrm{b}}/\Delta_{\mathrm{bc}}\}^{\mathrm{T}}.$$

The cohesive elements defined above act as follows ((a)–(c)):

(a) A cohesive element acts as a penalty element, maintaining the continuity of displacement at the element interface while $s = s_{\mathrm{ini}}$.

(b) The residual-strength parameter and the traction become small according to the relative displacement once the cohesive element is stressed beyond its strength ($0 < s < s_{\mathrm{ini}}$).

(c) Cohesive elements generate a crack surface completely when they absorb energy equal to the critical energy release rate ($s = 0$).

Next, we present the formulation for a finite-element analysis with cohesive elements. The virtual work for the analytical region V including the cohesive zone S_{coh} is as follows:

$$\int_V \boldsymbol{\sigma} : \delta\mathbf{E}\,\mathrm{d}V + \int_{S_{\mathrm{coh}}} \mathbf{T} \cdot \delta\boldsymbol{\Delta}\,\mathrm{d}S = \int_{S_{\mathrm{t}}} \mathbf{f} \cdot \delta\mathbf{u}\,\mathrm{d}S. \tag{4}$$

Here, $\boldsymbol{\sigma}$ is the stress tensor, $\mathbf{E}$ is the strain tensor, $\mathbf{u}$ is the displacement vector,

Downloaded by [Siauliu University Library] at 06:51 17 February 2013

f is the external force vector on the prescribed boundary S_t, and δ is the virtual component. The following relationship is obtained for the relative displacement $\boldsymbol{\Delta}$:

$$\boldsymbol{\Delta} = \begin{Bmatrix} \Delta_\mathrm{n} \\ \Delta_\mathrm{t} \\ \Delta_\mathrm{b} \end{Bmatrix} = \begin{bmatrix} 0 & 0 & -1 & 0 & 0 & 0 & 0 & 1 & 0 & 0 \\ -1 & 0 & 0 & \frac{t_\mathrm{l}}{2} & 0 & 1 & 0 & 0 & \frac{t_\mathrm{u}}{2} & 0 \\ 0 & -1 & 0 & 0 & \frac{t_\mathrm{l}}{2} & 0 & 1 & 0 & 0 & \frac{t_\mathrm{u}}{2} \end{bmatrix} \begin{Bmatrix} \hat{\mathbf{u}}_\mathrm{l} \\ \hat{\mathbf{u}}_\mathrm{u} \end{Bmatrix} = \mathbf{L} \begin{Bmatrix} \hat{\mathbf{u}}_\mathrm{l} \\ \hat{\mathbf{u}}_\mathrm{u} \end{Bmatrix}, \tag{5}$$

$$\hat{\mathbf{u}} = \{\, \hat{u} \quad \hat{v} \quad \hat{w} \quad \theta_x \quad \theta_y \,\}^\mathrm{T}.$$

Here, t_l and t_u are the thicknesses of the lower and upper layer of delamination. The displacement vector of element $\{\, \hat{\mathbf{u}}_\mathrm{l} \quad \hat{\mathbf{u}}_\mathrm{u} \,\}^\mathrm{T}$ is calculated from shape functions N^i and nodal displacement vector $\hat{\mathbf{U}}_e$:

$$\begin{Bmatrix} \hat{\mathbf{u}}_\mathrm{l} \\ \hat{\mathbf{u}}_\mathrm{u} \end{Bmatrix} = \begin{bmatrix} \mathbf{N}^1 & \mathbf{N}^2 & \mathbf{N}^3 & \mathbf{N}^4 & \mathbf{0} & \mathbf{0} & \mathbf{0} & \mathbf{0} \\ \mathbf{0} & \mathbf{0} & \mathbf{0} & \mathbf{0} & \mathbf{N}^1 & \mathbf{N}^2 & \mathbf{N}^3 & \mathbf{N}^4 \end{bmatrix} \hat{\mathbf{U}}_e = \mathbf{N}_\mathrm{coh} \hat{\mathbf{U}}_e, \tag{6}$$

$$\mathbf{N}^i = N^i \mathbf{I}_5, \quad \mathbf{I}_5 : \text{unit matrix } (5 \times 5),$$

$$\hat{\mathbf{U}}_e = \{\, \hat{\mathbf{U}}_\mathrm{l}^1 \quad \hat{\mathbf{U}}_\mathrm{l}^2 \quad \hat{\mathbf{U}}_\mathrm{l}^3 \quad \hat{\mathbf{U}}_\mathrm{l}^4 \quad \hat{\mathbf{U}}_\mathrm{u}^1 \quad \hat{\mathbf{U}}_\mathrm{u}^2 \quad \hat{\mathbf{U}}_\mathrm{u}^3 \quad \hat{\mathbf{U}}_\mathrm{u}^4 \,\}^\mathrm{T}.$$

With the above details, the matrix form of virtual work principal can be represented by

$$\delta \hat{\mathbf{U}}^\mathrm{T} \mathbf{K} \hat{\mathbf{U}} = \delta \hat{\mathbf{U}}^\mathrm{T} \mathbf{f}, \tag{7}$$

$$\mathbf{K} = \mathbf{K}_\mathrm{M} + \mathbf{K}_\mathrm{coh}, \tag{8}$$

$$\mathbf{K}_\mathrm{M} = \int_{V_\mathrm{M}} \mathbf{B}_\mathrm{M}^\mathrm{T} \mathbf{D}_\mathrm{M} \mathbf{B}_\mathrm{M} \, \mathrm{d}V, \tag{9}$$

$$\mathbf{K}_\mathrm{coh} = \int_{S_\mathrm{coh}} \mathbf{N}_\mathrm{coh}^\mathrm{T} \mathbf{L}^\mathrm{T} \bar{\mathbf{D}}_\mathrm{coh} \mathbf{L} \mathbf{N}_\mathrm{coh} \, \mathrm{d}S, \tag{10}$$

where $\hat{\mathbf{U}}$ is the nodal displacement vector; **f** is the external force vector; and **K**, **B** and **D** are the stiffness matrix, strain–displacement matrix and constitutive coefficients. Suffixes M and coh denote the Mindlin plate elements and the cohesive element.

Equation (7) is nonlinear since the stiffness matrix of cohesive elements $\mathbf{K}_\mathrm{coh}$ varies with the relative displacement. We used a direct-iteration method [11] to solve the nonlinear equation.

Downloaded by [Siauliu University Library] at 06:51 17 February 2013

2.2. Fatigue Law in Cohesive Elements

In this study, the concept of damage mechanics proposed by Kachanov is introduced to express the effect of cyclic loading. The following equation is applied for the residual strength parameter s of cohesive elements in the damage process zone:

$$\frac{\mathrm{d}s}{\mathrm{d}N} = -\alpha \frac{F^{\beta}}{s^{\gamma}}, \tag{11}$$

$$F = \sqrt{\left(\frac{\tau_{\mathrm{n}}}{\tau_{\mathrm{n\,max}}}\right)^2 + \left(\frac{\tau_{\mathrm{t}}}{\tau_{\mathrm{t\,max}}}\right)^2 + \left(\frac{\tau_{\mathrm{b}}}{\tau_{\mathrm{b\,max}}}\right)^2}.$$

Here, a dimensional parameter F is introduced to express the stress state at the crack tip. N denotes the number of cycles.

2.3. Calculation of Titanium Crack Growth Rate Using VCCT

Cracking in the titanium layer was assumed to occur from the hole and propagate perpendicular to the loading direction as in Fig. 1. An initial crack (0.2 mm) was introduced at the hole edge. The energy release rate G in the titanium layer is calculated using the VCCT with:

$$G = \frac{f_x \Delta_0}{t \Delta a_0}, \tag{12}$$

where f_x is the nodal force at the crack tip, t is the thickness of the titanium layer, Δ_0 is the crack opening displacement one node behind the crack tip, and Δa_0 is the element size ahead of the crack tip. The stress intensity factor K is related to the energy release rate and the titanium modulus E in the plane stress condition using

$$K = \sqrt{EG}. \tag{13}$$

The crack growth rate in the titanium layer is expressed using Paris' law:

$$\frac{\mathrm{d}a}{\mathrm{d}N} = C(\Delta K)^{\mathrm{m}}. \tag{14}$$

3. Application to Experiments

3.1. Overview of Experiments

This section introduces the fatigue experiments for open-hole Ti/GFRP cross-ply laminates conducted by one of the authors [8]. Ti/GFRP laminates consist of a 140 μm thickness titanium-alloy sheet bonded together with autoclaved GFRP cross-ply laminates $[0_4/90_8]_{\mathrm{s}}$, and CW-tape (GE380G135SBEMQWS, Mitsubishi Rayon Co. Ltd.). Epoxide-based adhesive (DP-460, Sumitomo 3M Co. Ltd.) was used to bond the titanium layer and GFRP. The test specimens were 200 × 40 mm rectangular coupons and about 3.10 mm thick. A circular hole with a diameter of 6 mm was drilled in the center of the specimens. Constant-amplitude fatigue testing was conducted using a servo-hydraulic testing machine, an Instron 8801, with

Downloaded by [Siauliu University Library] at 06:51 17 February 2013

a frequency of 5 Hz and a stress ratio of $R = 0.1$. The maximum applied stress was 71.4 MPa, which is 30% of the tensile strength of the Ti/GFRP laminates.

Scanned images of the specimen after 10 000, 30 000 and 400 000 cycles of supersonic scanning may be seen in Fig. 4(a–c). At 10 000 cycles, a transverse crack

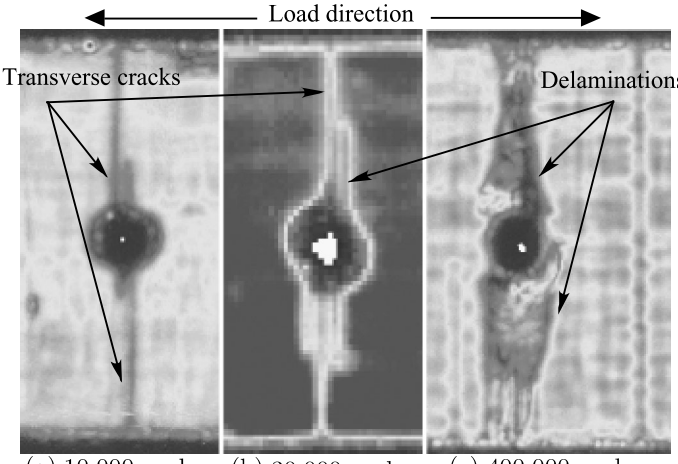

(a) 10,000 cycles (b) 30,000 cycles (c) 400,000 cycles

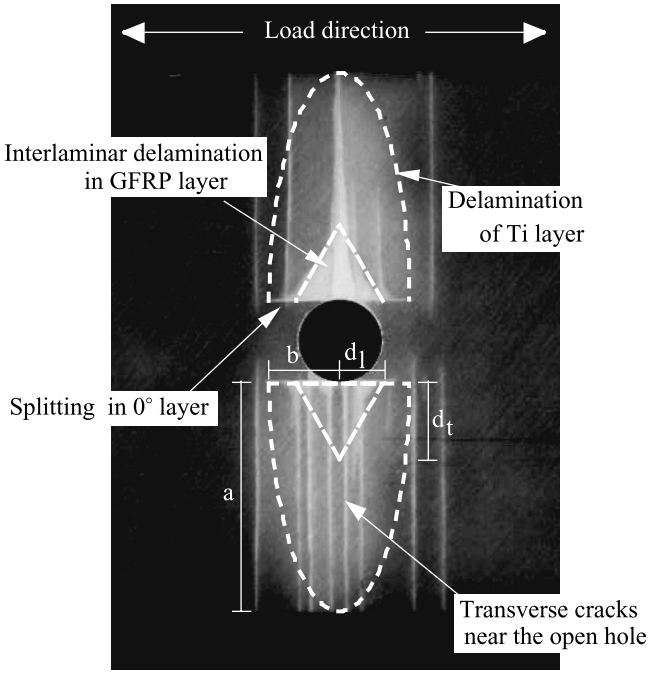

(d) Detailed damage observation

Figure 4. (a)–(c): Images of Ti/GFRP specimens captured by an ultrasonic flaw detector. (d): Damage observation of GFRP layers in Ti/GFRP after fatigue loading (Ti layer was removed).

Downloaded by [Siauliu University Library] at 06:51 17 February 2013

Table 1.
Profile and maximum size for each damage mode

Damage modes	Profile	Edge	Size (mm)
Ti/GFRP	ellipse	a (= crack length)	17
Delamination		b	6
0°/90°	triangle	d_t	8
Delamination		d_l	4

Downloaded by [Siauliu University Library] at 06:51 17 February 2013

in 90° plies had propagated completely across the ligaments but delamination at the Ti/GFRP interface was not yet visible (Fig. 4(a)). At 30 000 cycles, the titanium cracks and titanium/GFRP delamination are visible only near the hole (Fig. 4(b)). After the titanium crack penetrated the ligaments at about 200 000 cycles, Ti/GFRP delamination was widely propagated after 400 000 cycles.

Although the outline of fatigue-damage behavior is demonstrated by supersonic scanning, the detailed size and profile of the delamination and matrix cracking are not visible. Therefore the interlayer damage of the Ti/GFRP laminates was observed by peeling the titanium layer away (Fig. 4(d)). As seen in Fig. 4, delamination at the Ti/GFRP interface was in an elliptical shape, with the major axis being the titanium crack length and the minor axis the split length. Transverse cracks appeared in the region near the hole, and triangular delamination appeared in the region near the hole between the 0° and the 90° plies. The average damage sizes when the titanium crack penetrated the specimen are listed in Table 1.

Fatigue-damage behavior in open-hole Ti/GFRP laminates may be summarized as follows: First, transverse cracks appear from the region near the hole in GFRP early in the fatigue life. A crack in the titanium layer then propagates from the hole edge. Following that, cracking in the titanium layer and elliptical delamination at the Ti/GFRP interfaces propagate as the number of cycles increases. 0° ply splitting and triangular delamination at the 0°/90° ply interfaces also progress with increasing numbers of cycles.

3.2. Simulation Result

Fatigue crack-growth simulation for open-hole monolithic titanium specimens was carried out to estimate the Paris' law parameter (equation (14), C and m) by comparing the crack growth with results of experiments conducted by Oki [12]. The test specimens were 200 × 40 mm rectangular coupons with a circular hole in the center with a radius of 3 mm. The stress ratio was $\mathbf{R} = 0.1$ and the maximum stress level was 270.6 MPa, which corresponds to the maximum stress levels in the titanium layer in the fatigue simulation for Ti/GFRP laminates. The simulation result, with Paris' law parameters $C = 2.1 \times 10^{-7}$ and $m = 2.6$, fitted well with the experimental result (Fig. 6).

Table 2.
Material properties of titanium alloy and GFRP

(a) Titanium alloy	
Young's modulus (GPa)	85.9
Poisson's ratio	0.38
(b) GFRP	
Longitudinal Young's modulus (GPa)	36.9
Transverse Young's modulus (GPa)	10
In-plane shear modulus (GPa)	3.3
Out-of-plane shear modulus (GPa)	3.6
In-plane Poisson's ratio	0.32
Out-of-plane Poisson's ratio	0.49

Downloaded by [Siauliu University Library] at 06:51 17 February 2013

Table 3.
Properties of the cohesive elements

	$\tau_{\mathrm{n\,max}}$ (MPa)	$\tau_{\mathrm{t\,max}}, \tau_{\mathrm{b\,max}}$ (MPa)	G_{Ic} (J/m^2)	$G_{\mathrm{IIc}}, G_{\mathrm{IIIc}}$ (J/m^2)	Fatigue parameter		
					A	β	γ
Split	40	65	250	720	2×10^{-5}	1.5	1.5
0°/90° delamination	40	65	250	720	1×10^{-5}	1.5	1.5
Ti/GFRP delamination	40	60	210	450	1×10^{-4}	1.5	1.5

Fatigue simulations were then conducted for open-hole Ti/GFRP laminates using the same specimen as used in the experiment introduced in Section 3.1. The material properties used in the simulation are summarized in Table 2. The parameters for cohesive elements are listed in Table 3. The finite-element model used in the analysis is depicted in Fig. 1. The respective thicknesses of the 0° ply and 90° ply were 0.444 mm and 0.888 mm. In this study, cohesive elements were introduced to represent the occurrence and extension of delamination and 0° ply splits. Splits are expressed by cohesive elements located in the 0° ply from the hole toward the load direction. Cohesive elements were also inserted into all ply interfaces to represent delamination. It was confirmed that transverse cracks propagated across the specimen before cracks appeared in the titanium layer. A transverse crack is preliminarily set up by eliminating the symmetric boundary condition at the edge of the 90° layer. Thermal residual stresses for the temperature change ($\Delta T = -93$ K) were also considered.

Figure 5 illustrates the change in delamination area with respect to the ratio of the number of cycles to the failure life. Here, we defined failure as the penetration of the titanium crack. The delamination shape at the Ti/GFRP interface is elliptical, such that the major axis is the titanium crack length and the minor axis is the split length.

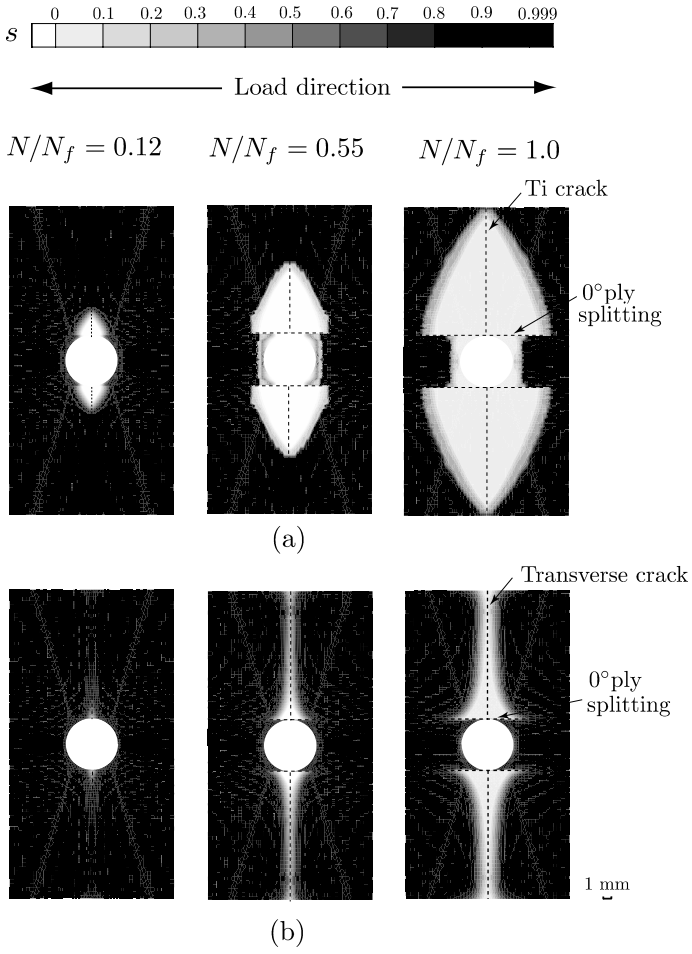

Figure 5. Predicted fatigue-damage progress in Ti/GFRP laminates. (a) Ti/GFRP interface. (b) 0°/90°ply interface.

Meanwhile, delamination at the 0°/90° interface propagates with a triangular shape. These results agree well with the experiment.

The predicted and experiment fatigue-crack growth in the titanium layer and in monolithic titanium are plotted in Fig. 6. The crack growth rate in monolithic titanium increases exponentially, while that in the titanium layer of Ti/GFRP laminates gradually slows down during the initial stage and becomes constant in the middle of the fatigue simulation. It is worthy of special mention that we used the same parameter value in Paris' law for both monolithic titanium and the titanium layer of the Ti/GFRP laminates.

We were able to confirm that the crack growth rate of the titanium layer and the delamination shape at the interface of the Ti/GFRP and 0°/90° layers agreed with the experiment results as described above.

Downloaded by [Siauliu University Library] at 06:51 17 February 2013

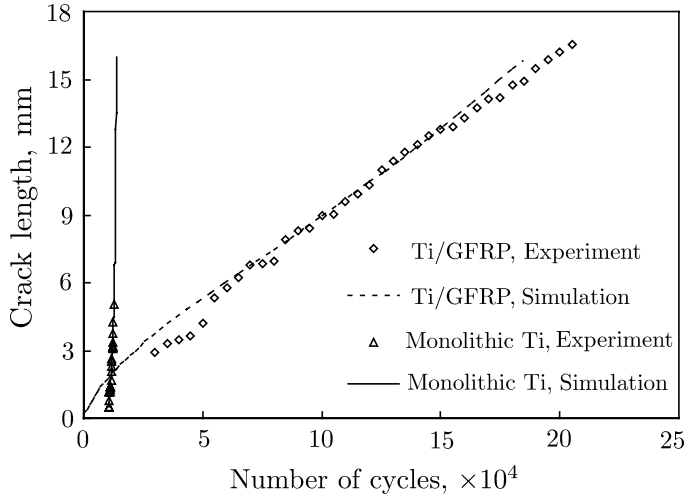

Figure 6. Comparison between crack-growth curves for monolithic titanium and Ti/GFRP.

Complementary analysis was performed without considering the residual stresses ($\Delta T = 0$ K). In this case, the delamination at the 0°/90° interface is smaller than the result with the residual stress. The crack growth rate was approximately 33 percent lower than the result with the residual stresses. In contrast, the delamination at the Ti/GFRP interface was almost the same as the result with the residual stresses.

3.3. Effect of Changing the Parameters of Cohesive Elements on Fatigue Damage Progress

In this section, we discuss the effects of changing the parameters of cohesive elements, which express the delamination at Ti/GFRP interfaces or the splitting in GFRP, on the delamination shape and the crack-growth rate of the titanium layer. Here, we assume the value of the strength parameter that was used in Section 3.2, i.e., $\tau_{i\,\max 0}$, and let it range from 0.5 times to 1.5 times $\tau_{i\,\max 0}$ as a parameter. We omit the effect of the critical energy release rate G_{ic} because it does not significantly affect the delamination profile or the crack-growth rate.

The effect of varying the strength of the Ti/GFRP interface on delamination shape is illustrated in Fig. 7. A decrease in strength $\tau_{i\,\max}$ spreads the delaminated region near the titanium layer crack tip. The effect of varying the strength of the Ti/GFRP interface on crack growth in the titanium layer is seen in Fig. 8. The strength $\tau_{i\,\max}$ of the interface affects the crack growth in the titanium layer. An increase in strength decreases the rate of crack growth.

Meanwhile, delamination shapes are presented in Fig. 9 with a variety of strengths for the cohesive elements at the 0° ply splits. The strength of the Ti/GFRP interface did not change then. *A* decrease in strength $\tau_{i\,\max}$ increases the splitting growth, which leads to an increase in the delaminated area along the splitting. Therefore, the overall shape of the delaminated region appears to be triangular (a)

Downloaded by [Siauliu University Library] at 06:51 17 February 2013

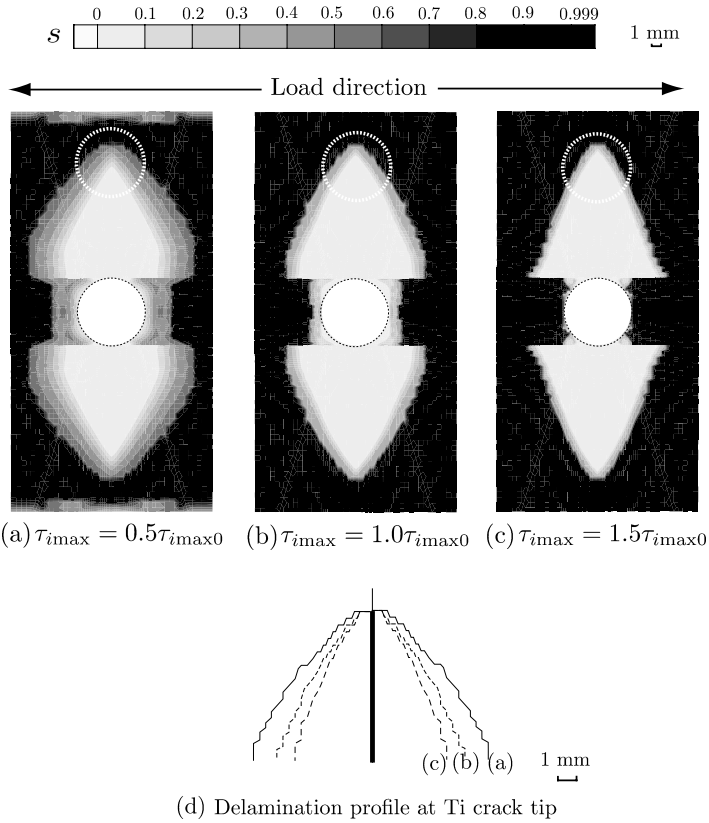

Figure 7. Effect of changing the parameters of cohesive elements for Ti/GFRP interface on delamination profile.

or elliptical (c). However, little effect in the delamination shape is observed at the region near the titanium crack tip (Fig. 9(d)). This leads to a smaller effect on the crack-growth rate in the titanium layer (Fig. 10).

The results given in this section clarify that the strength at the Ti/GFRP interface determines the delamination shape and becomes a factor governing the crack growth rate when the applied stress amplitude is constant. Burianek *et al.* [5] have modeled delamination as being triangular or elliptical. However, the overall shape of the delamination is not an important factor in predicting the crack growth rate, though it is suggested by our simulation that the crack growth rate is correlated with the delamination shape near the crack tip.

4. Conclusions

A new numerical approach for predicting fatigue damage progress in FML (Ti/GFRP cross-ply laminates) using a finite-element method was proposed. This model expresses the damage in FML (0° ply splits and delamination at Ti/GFRP

Downloaded by [Siauliu University Library] at 06:51 17 February 2013

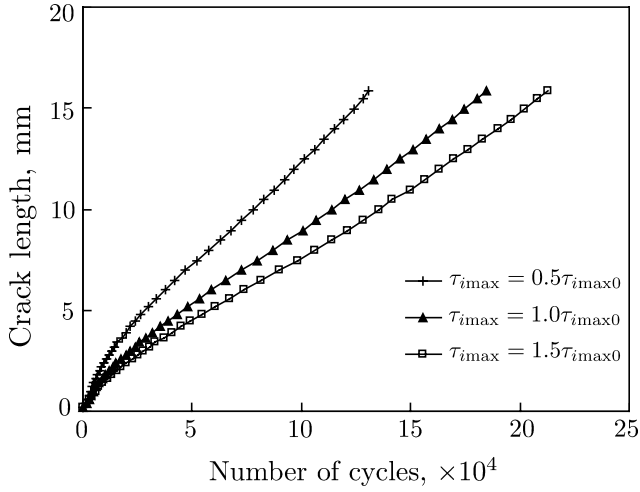

Figure 8. Effect of changing the parameters of cohesive elements for Ti/GFRP interface on Ti crack growth.

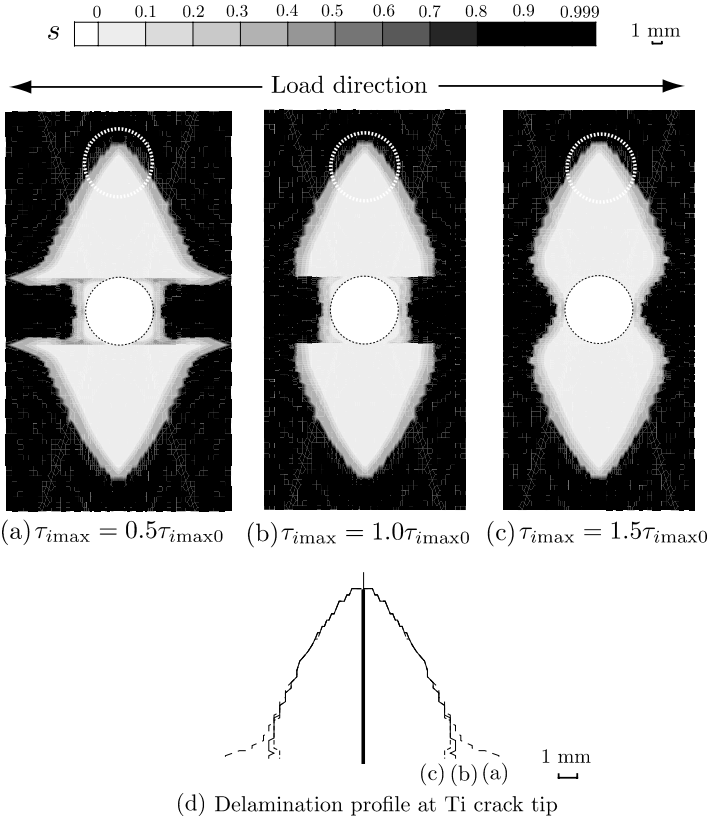

Figure 9. Effect of changing the parameters of cohesive elements for split on delamination profile.

Downloaded by [Siauliu University Library] at 06:51 17 February 2013

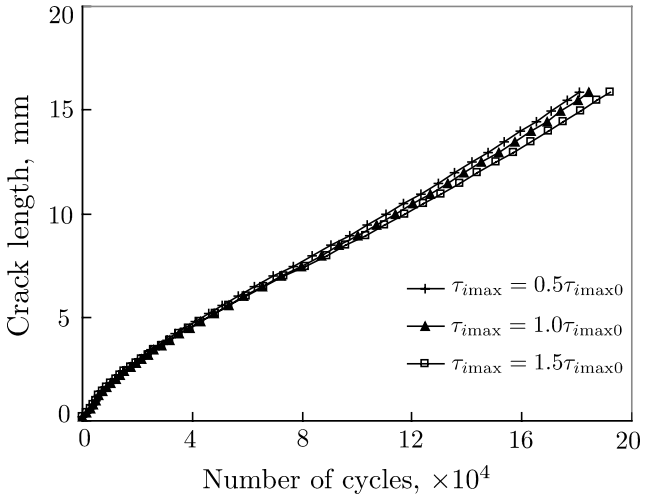

Figure 10. Effect of changing the parameters of cohesive elements for split on Ti crack growth.

interfaces and 0°/90° ply interfaces) with cohesive elements. A fatigue law was introduced into the cohesive elements to represent the effects of cyclic loading. The simulation results (fatigue crack growth rate in the titanium layer, delamination shape, and size at the Ti/GFRP and 0°/90° interfaces) agreed well with the experimental results obtained by one of the authors.

Additional study was conducted on the effects of changing the parameters of the cohesive elements on the delamination shape and the crack growth rate of the titanium layer. The results indicated that the strength at the Ti/GFRP interface determines the delamination shape, and that strength is a major factor in the crack growth rate in the titanium layer.

Acknowledgement

The authors acknowledge the support of the Ministry of Education, Culture, Sports, Science and Technology of Japan under Grants-in-Aid for Scientific Research (No. 18360406).

References

1. L. B. Vogelesang and A. Vlot, Development of fibre metal laminates for advanced aerospace structures, *J. Mater. Proc. Technol.* **103**, 1–5 (2000).
2. J. Sinke, Development of fiber metal laminates: concurrent multi-scale modeling and testing, *J. Mater. Sci.* **41**, 20, 6777–6788 (2006).
3. A. Asundi and A. Y. N. Choi, Fiber metal laminates: an advanced material for future aircraft, *J. Mater. Proc. Technol.* **63**, 384–394 (1997).
4. D. W. Rhymer and W. S. Johnson, Fatigue damage mechanisms in advanced hybrid titanium composite laminates, *Intl J. Fatigue* **24**, 995–1001 (2002).

Downloaded by [Siauliu University Library] at 06:51 17 February 2013

5. D. A. Burianek, A. E. Giannakopoulos and S. M. Spearing, Modeling of face-sheet crack growth in titanium–graphite hybrid laminates Part I, *Engng Fract. Mech.* **70**, 775–798 (2003).
6. D. A. Burianek and S. M. Spearing, Fatigue damage in titanium–graphite hybrid laminates, *Compos. Sci. Technol.* **62**, 607–617 (2002).
7. D. A. Burianek and S. M. Spearing, Modeling of face-sheet crack growth in titanium–graphite hybrid laminates, Part II, *Engng Fract. Mech.* **70**, 799–812 (2003).
8. H. Nakatani, K. Osaka, T. Kosaka, Y. Sawada and T. Okabe, Crack growth behavior of open-hole specimens of Ti/GFRP laminates under fatigue loading, in: *Proc. JCOM-37*, Japan, pp. 230–234 (2008).
9. J. Skrzypek and A. Ganczarski, *Modeling of Material Damage and Failure of Structures*. Springer-Verlag, Berlin, Germany (1999).
10. P. H. Geubelle and J. S. Baylor, Impact-induced delamination of composites: a 2D simulation, *Composites Part B* **29**, 589–602 (1998).
11. D. R. J. Owen and E. Hinton, *Finite Elements in Plasticity*. Pineridge Press, Swansea, UK (1980).
12. J. Oki, Tensile fatigue damage behavior of Ti/GFRP open hole specimen, *BS Thesis*, Department of Engineering, Osaka City University, Japan (2007).

Downloaded by [Siauliu University Library] at 06:51 17 February 2013